

Journal of Materials Chemistry A

Accepted Manuscript



This is an *Accepted Manuscript*, which has been through the Royal Society of Chemistry peer review process and has been accepted for publication.

Accepted Manuscripts are published online shortly after acceptance, before technical editing, formatting and proof reading. Using this free service, authors can make their results available to the community, in citable form, before we publish the edited article. We will replace this *Accepted Manuscript* with the edited and formatted *Advance Article* as soon as it is available.

You can find more information about *Accepted Manuscripts* in the [Information for Authors](#).

Please note that technical editing may introduce minor changes to the text and/or graphics, which may alter content. The journal's standard [Terms & Conditions](#) and the [Ethical guidelines](#) still apply. In no event shall the Royal Society of Chemistry be held responsible for any errors or omissions in this *Accepted Manuscript* or any consequences arising from the use of any information it contains.

Intelligent Rubber with Tailored Properties for Self-healing and Shape Memory

Dong Wang,^{ab} Jing Guo,^{ab} Huan Zhang,^{ab} Beichen Cheng,^a Heng Shen,^{ab} Ning Zhao^{*a} and Jian Xu^{*a}

^a*Beijing National Laboratory for Molecular Sciences, Institute of Chemistry, Chinese Academy of Sciences, Beijing, 100190, China. E-mail: zhaoning@iccas.ac.cn; jxu@iccas.ac.cn*

^b*University of Chinese Academy of Sciences, Beijing 100049, China*

† Electronic Supplementary Information (ESI) available. See DOI: 10.1039/b000000x/

ABSTRACT: A strategy of combining covalent and non-covalent cross-links to construct multifunctional rubber materials with intelligent self-healing and shape memory ability is demonstrated. The rubbers were prepared by self-assembly of complementary polybutadiene oligomers bearing carboxylic acid and amine groups through reversible ionic hydrogen bonds via acid-base reaction, and then further covalently cross-linking by tri-functional thiol via thiol-ene reaction. The resulting polymers exhibit self-healing and shape memory functions owing to the reversible ionic hydrogen bonds. The covalent cross-linking density can be tuned to achieve tailorable mechanical and stimuli-responsive properties: a low covalent cross-linking density remains the rubber remarkable self-healing capability at ambient temperature without any external stimulus, while a high covalent cross-linking density improves the mechanical strength and induces shape memory behavior, but effective self-healing needs to be triggered at high temperature. This strategy might open a promising pathway to fabricate intelligent multifunctional polymers with versatile functions.

KEYWORDS: intelligent rubber; polybutadiene; ionic hydrogen bonds; self-healing; shape memory

1 Introduction

Non-covalent interactions, such as hydrogen bonding, metal-ligand coordination, π - π stacking, hydrophobic interactions and host-guest interactions, have been utilized to construct supramolecular polymers.¹⁻⁵ Compared to the strong, nonreversible covalent bonds, the weak non-covalent bonds are generally stimuli-responsive, that is, they exhibit reversible association-dissociation behavior on exposure to external stimulus such as light, heat or chemicals. These reversible behaviors endow supramolecular polymers with versatile functions, such as facile processing/recycling,^{6,7} self-healing,⁸⁻¹² shape memory¹³⁻¹⁹ and high responsivity to stimuli.²⁰⁻²⁴ Nowadays, there is an increasing need to develop multifunctional polymers that can serve some certain purposes by the combination of various predefined functions. Based on the smart “switchable” shape behavior of shape memory polymers when exposed to external stimuli, multifunctional polymers showing electroactive²⁵⁻²⁷ or magnetoactive^{28, 29} shape memory effect, or combining shape memory behavior with other different functionalities, such as degradability,^{30,31} controlled drug release,³² thermochromism^{33,34} and self-healing,³⁵⁻⁴⁰ have been developed in recent years. For example, the shape memory behavior could assist the healing process by bringing fractured surfaces together and the self-healing ability could also improve the lifetime of shape memory polymers. Because of the complementary properties of the weak, reversible non-covalent bonds and the strong, nonreversible covalent bonds, the combination of non-covalent and covalent cross-links is a promising approach to fabricate functional polymers with tailored mechanical properties and stimuli-responsive behaviors.⁴¹⁻⁴⁸ However, the co-existence of the two types of cross-links may give rise to conflicting properties, and it is still a challenge to integrate multiple functionalities such as self-healing and shape memory properties with good mechanical performance into a single component material.

Ionic hydrogen bond is a particular type of hydrogen bond with potential proton transfer between organic cations (eg. primary or secondary amine, quaternary ammonium) and anions (eg. carboxylates,

sulfates).^{49,50} These bonds are usually formed by mixing acid and base, *i.e.* the classical acid-base reaction.^{51,52} Besides, amidinium carboxylate or sulfonate ion pairs generally formed between organic cations and anions are also defined as ionic interactions in some reports.^{4, 53-55} In recent years, this type of reversible non-covalent interaction has been used to construct supramolecular systems.⁵³⁻⁵⁹ Pioneering works by Matsushita and coworkers described a simple preparation of supramolecular polymer by mixing carboxy-terminated telechelic polymers (PEA-(COOH)₂, PDMS-COOH) with PEI, a multi-amino polymer.^{57,58} Considering its high stability and facile accessibility, ionic hydrogen bonding holds promise for the facile fabrication of multifunctional polymers.

We present a new thermal-reversible rubber constructed by thiol-ene functionalized polybutadiene (PBs) via a combination of dynamic ionic hydrogen bonds and covalent cross-links. PB was chosen due to its high density of vinyl bonds enable the facile accessibility of crosslinking and chemical modification via thiol-ene reaction,^{60,61} which is a highly efficient route to quantitatively introduce a variety of functional groups on the polymer chain. Herein, low molecular weight PB was functionalized separately with amine and carboxylic acid groups via thiol-ene reaction to obtain two complementary oligomers, namely PB-COOH and PB-NH₂. When mixed, PB-COOH and PB-NH₂ were assembled by the formation of ionic hydrogen bonds which are in the form of amidinium carboxylate ion pairs. Incorporation of covalent cross-links can be achieved by further photo-cross-linking the PB chains with tri-functional thiol via thiol-ene reaction. By adjusting the covalent cross-linking density, the resulting polymers can achieve tailored mechanical and stimuli-responsive properties, including self-healing and shape memory functions.

2 Experimental Section

2.1 Materials

Polybutadiene (PB, 90% 1, 2-addition, $M_w=9.4\times 10^3$, PDI=1.15), trimethylolpropane tris (3-mercaptopropionate) (TMPT, ≥ 95.0), 3-mercaptopropionic acid (3TPA, $\geq 99\%$), cysteamine ($\sim 95\%$), 2, 2-dimethoxy-2-phenylacetophenone (DMPAP, 99%) were purchased from Sigma-Aldrich and used without further purification.

2.2 Synthesis of PB-COOH

To a stirred solution of PB (5.0 g) in CH_2Cl_2 (25 mL), 3TPA (0.98 g) and DMAP photoinitiator (0.02 g) were added. The amount of 3TPA was calculated by the molar ratio of 1:10 to the total amount of PB monomer units, namely, the concentration of carboxylic acid groups along PB backbone is 10 mol%. The reaction mixture was then irradiated by a 365 nm mercury lamp (light intensity= 85 mW cm^{-2}) for 4 h at room temperature under stirring. After UV irradiation, the polymer solution was washed with brine for three times to remove the unreacted 3TPA and then the solvent was removed under reduced pressure to give viscous PB-COOH. The actual concentration of carboxylic acid groups along PB backbone calculated from the ^1H NMR spectra is about 9.2 mol% (mole fraction relative to the total number of PB monomer units).

2.3 Synthesis of PB-NH₂

To a stirred solution of PB (5.0 g) in CH_2Cl_2 (25 mL), a solution of cysteamine (0.71 g) and DMAP photoinitiator (0.02 g) dissolved in $\text{CH}_2\text{Cl}_2/\text{CH}_3\text{CH}_2\text{OH}$ (10/1 v/v) (25 mL) was added. Here $\text{CH}_3\text{CH}_2\text{OH}$ was used because of the low solubility of cysteamine in CH_2Cl_2 . The amount of cysteamine was calculated by the molar ratio of 1:10 to the total amount of PB monomer units, namely, the concentration of amine groups along PB backbone is 10 mol%. The reaction mixture was then irradiated by a 365 nm mercury lamp (light intensity= 85 mW cm^{-2}) for 4 h at room temperature under stirring. After UV irradiation, the polymer solution was washed with brine for three times to remove the unreacted cysteamine and then the solvent was removed under reduced pressure to give viscous PB-NH₂. The actual

concentration of amine groups along PB backbone calculated from the ^1H NMR spectra is about 9.4 mol% (mole fraction relative to the total number of PB monomer units).

2.4 Preparation of PB-COOH/ NH_2 Supramolecular Polymers

The equimolar PB-COOH (2.99 g) and PB- NH_2 (2.85 g) were dissolved separately in CH_2Cl_2 at a concentration of 20% w/v. Then the PB- NH_2 solution was added dropwise to the stirred PB-COOH solutions in a round-bottom flask, and the mixture was allowed to stir for another 12 h to ensure complete acid-base reaction. The solution was cast into a Teflon dish, allowed to evaporate the solvent at room temperature, and further dried in vacuum. A soft supramolecular PB film was obtained.

2.5 Photo-Cross-Linking of the Polymers

To a stirred solution of PB-COOH/ PB- NH_2 dissolved in CH_2Cl_2 , a solution of trithiol cross-linker TMPT (0, 2, 6 wt %) and DMAP photoinitiator dissolved in 10 mL CH_2Cl_2 was added. After stirring for 30 min, the solution was cast into a Teflon dish, and the solvent was allowed to evaporate slowly to produce a film. Caution must be taken to protect the mixtures from any sources of light before it had been cast into a film. Finally, the film was irradiated using a 365 nm mercury lamp (light intensity=85 mW cm^{-2}) for 1 h on each side to complete the cross-linking reactions.

2.6 Characterization

Wide angle X-ray diffraction (WAXD) measurements were carried out at room temperature on flat polymer films (length 10mm \times width 10 mm \times thickness 0.3mm) using a Micscience M-18XHF (with CuK α radiation) instrument. The scanning range of the Bragg $2q$ angle varied from 3 to 60° under a scanning rate of 5°/min. Fourier transform infrared (FTIR) spectra were recorded on a Perkin-Elmer 2000 FT-IR spectrophotometer with a disc of KBr. ^1H NMR spectra were carried out on a Bruker 400 M instrument with TMS as an internal standard and CDCl_3 as solvent.

Thermal characterization was performed on a TA Instrument Q2000 differential scanning calorimeter

(DSC) to determine glass transition temperature, T_g . Samples were heated from -90 to 100 °C at a rate of 10 °C /min under a nitrogen atmosphere. For each sample, two cooling-heating runs were performed and the data were obtained from the second heating curves.

Rheology measurements were performed on an AR-2000ex rheometer (TA Instruments, USA) with an 8-mm parallel plate. Oscillatory frequency sweep experiments were carried out from 100 to 0.01 rad s^{-1} with a strain in the linear region at 20 °C. Rheological thermal cycling experiments were conducted with a temperature range of -30-60 °C at $\omega = 10$ rad s^{-1} , $\gamma = 0.03\%$ from -30 to -10 °C and $\gamma = 0.1$ from -10 to 60 °C. The temperature ramp rate was 3 °C/min on heating and cooling cycles.

The tensile mechanical properties of the polymers were measured in tensile mode on a TA Instruments Q800 DMA. The samples were cut into rectangular films with approximate dimensions of 20 mm \times 4 mm \times 0.3 mm. Stress/strain tests were conducted in controlled force mode with a force rate of 3 N/min at room temperature (~ 20 °C). Each measurement was repeated at least three times and the values were averaged.

Self-healing Tests: For self-healing tests, a sample was cut into two separate pieces with a razor blade. The fracture surfaces were brought into contact together with a moderate press immediately. After healing at room temperature for certain time, the healed samples were then subjected to stress-strain tests at room temperature. Healing efficiency was calculated from the ratio of tensile strength of healed samples to that of the virgin samples.⁶² Each measurement was repeated at least three times and the values were averaged.

Shape Memory Characterization: Shape memory cycles of the polymers were performed using a TA Instruments DMA Q800 (tension film clamp, controlled force mode). The samples were cut into rectangular films with approximate dimensions of 20 mm \times 4 mm \times 0.3 mm. The testing program was set up as follows: (1) the film sample was first heated from room temperature to 60 °C with a preload force

of 0.001 N. After equilibrating at 60 °C for 5 min, the sample was stretched by a ramping stress; (2) the sample was then cooled to 10 °C at a rate of 3 °C/min and held at this temperature for 5 min under constant stress; (3) the stress was unloaded in 1 min and the sample was allowed to equilibrate for 3 min; (4) the sample is reheated to 60 °C at 3 °C/min, held at 60 °C for 5 min and cooled back to 10 °C. The thermomechanical cycle consisting of four steps is repeated five times on the same sample. The strain-fixing ratio (R_f) and the strain-recovery ratio (R_r) are commonly used to assess the efficiency of the shape-memory response, which are calculated using the following equations:⁶³

$$R_f = \frac{\varepsilon_u(N)}{\varepsilon_m(N)} \times 100\% \quad (1)$$

$$R_r = \frac{\varepsilon_m(N) - \varepsilon_p(N)}{\varepsilon_m(N) - \varepsilon_p(N-1)} \times 100\% \quad (2)$$

Where N denotes the number of cycles, $\varepsilon_m(N)$, $\varepsilon_u(N)$ and $\varepsilon_p(N)$ represent the maximum strain before unloading, the strain after unloading and the recovered strain at the N th cycle, respectively.

3 Results and Discussion

The preparation of the polymers is described in detail in the Experimental Section. Briefly, the low molecular weight PB was functionalized with 3TPA and cysteamine via thiol-ene reaction, respectively (Fig. 1a). The functionalized PB-COOH and PB-NH₂ oligomers were mixed in a 1:1 stoichiometry in solvent of CH₂Cl₂ to form a supramolecular PB-COOH/NH₂ based on ionic hydrogen bonding. Then a small amount of tri-functional thiol (TMPT) as covalent cross-linker was added, the solution was cast in a Teflon mold, and thiol-ene reaction was carried out under UV irradiation. The final product was consisted of both non-covalent and covalent cross-linking (Fig. 1b). Three polymers with different concentration of trithiol cross-linker of 0, 2 and 6 wt% were synthesized, which were termed as SPB-0%, SPB-2% and SPB-6%, respectively.

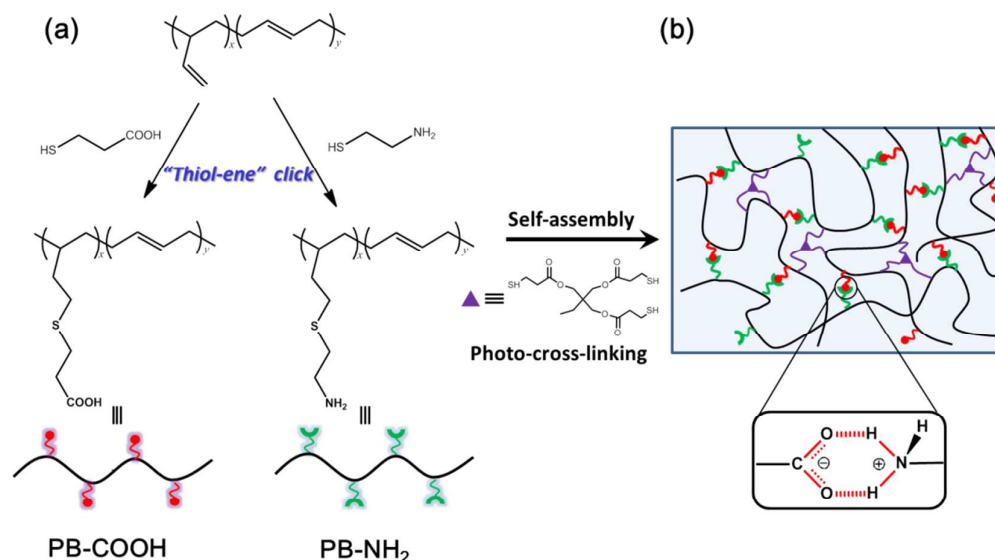


Fig. 1 (a) Synthetic route of PB-COOH and PB-NH₂. (b) Schematic illustration of polymer network containing both ionic hydrogen bonds and covalent cross-links. The ionic hydrogen bonds are formed by proton transfer reaction between carboxylic acid and amine groups.

The chemical structures of functionalized PB-COOH and PB-NH₂ oligomers were characterized with ¹H NMR and FT-IR. The typical ¹H NMR spectrum obtained from pristine PB, PB-NH₂ and PB-COOH are shown in Fig. 2a. Compared to the pristine PB, the occurrence of broad peaks at 2.4-2.7 ppm for both PB-NH₂ and PB-COOH, corresponding to the four methylene protons at the thioether linkage (CH₂-S-CH₂), confirms the success of thiol-ene coupling with cysteamine and 3TPA. The new signals at 2.8 ppm for PB-NH₂ and 2.9 ppm for PB-COOH can also be observed, which could be assigned to the methylene protons adjacent to amine groups (CH₂-NH₂) and carboxylic acid groups (CH₂-COOH), respectively. In addition, the degree of functionalization can be calculated by integration of peaks assigned to protons at the thioether linkage to determine the amounts of amine and carboxylic acid groups on the PB chains. The functionalization degrees of about 94% for PB-NH₂ and 92% for PB-COOH are obtained from the ¹H NMR data, showing the high efficiency of thiol addition. As a result, the concentrations of amine and carboxylic acid groups along PB backbone are determined to be 9.4 mol%

and 9.2 mol%, respectively. Fig. 2b shows the typical FTIR spectra of pristine PB, PB-NH₂, PB-COOH, and PB-COOH/NH₂. For PB-NH₂ and PB-COOH, the presence of absorbance at 3382 cm⁻¹ corresponding to -NH₂ stretching vibration and 1714 cm⁻¹ corresponding to C=O stretching vibration indicates the incorporation of amine and carboxylic acid groups into the PB backbone, respectively. For the prepared supramolecular polymer PB-COOH/NH₂, the peak at 1714 cm⁻¹ for neutral COOH almost completely disappears, and a new peak at 1570 cm⁻¹ emerges, which can be attributed to carboxylate anions arising from proton transfer reaction (acid-base reaction) between carboxylic acid groups on PB-COOH and amine groups on PB-NH₂, thus confirming the formation of ionic hydrogen bonds in the supramolecular polymers.

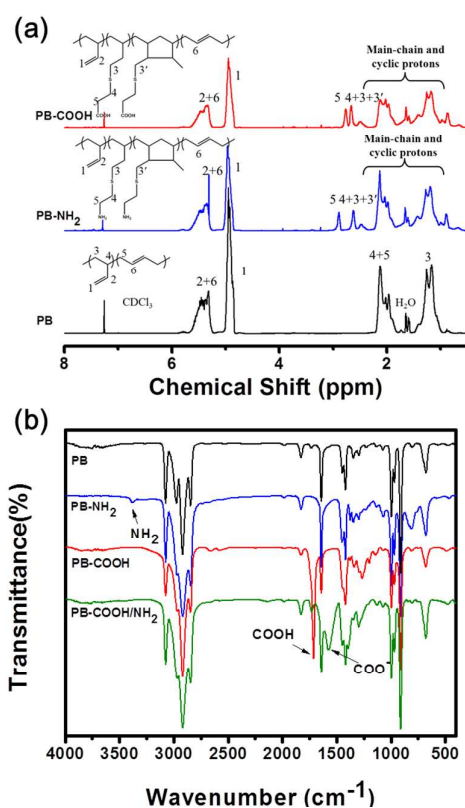


Fig. 2 (a) ¹H NMR spectra of PB, PB-NH₂ and PB-COOH in CDCl₃, (b) FTIR spectra of PB, PB-NH₂, PB-COOH and supramolecular polymer PB-COOH/NH₂.

The WXR D patterns of the three polymers (Fig. S1) only displayed a broad amorphous diffraction peak at the 2θ of 16° , suggesting that all the three polymers are amorphous. This can be further proved by the DSC results (Fig. 3a) as no crystalline peak was detected. The DSC thermograms show that the T_g increases from 1°C for SPB-0% to 10 and 15°C for SPB-2% and SPB-6%, respectively, due to the restriction of chain mobility by the formation of covalent cross-linking networks. The typical stress-strain curves at room temperature ($\sim 20^\circ\text{C}$) are shown in Fig. 3b. The SPB-0% showed the elongation at break over 400% with Young's modulus of 2.13 MPa, revealing comparable mechanical properties to conventional soft rubber due to the formation of ionic hydrogen bonding networks. The increase of the covalent cross-linking density leads to a remarkable improvement in mechanical strength but a decrease in the elongation at break. This indicates that the mechanical properties of the polymers can be systematically tuned by varying the cross-linking density. The key mechanical parameters of these three polymers are summarized in Table 1. It can be observed that the tensile stress at break increases by 2.5-fold from 1.02 to 2.52 MPa when the content of trithiol cross-linker changed from 0 to 6%, while the elongation at break decreases from 410 to 158%. This is because the ionic hydrogen bonds can reversibly break and re-form to rearrange the polymer chains along stretching direction, leading to the good extensibility, whereas covalent cross-links form an irreversible elastic network, which restricts the mobility of polymer chains, resulting in an enhanced mechanical strength but poor extensibility.

In addition, the dynamic viscoelastic properties of these polymers are investigated. The frequency dependence of storage modulus (G'), loss modulus (G'') and loss factor $\tan \delta$ (G''/G') of the polymers at 20°C is shown in Fig. 3c and 3d. The G' and G'' of SPB-2% and SPB-6% increased remarkably in comparison to those of SPB-0%, indicating that the incorporation of covalent cross-links can be of benefit for improving mechanical performance, whereas $\tan \delta$ decreases correspondingly. As shown in Fig. 3c, a transition from a viscoelastic liquid state with $G'' > G'$ to an elastic network state with $G' > G''$ can be also

observed with the increase of the frequency. At low frequencies, the supramolecular interactions are able to break and re-form at the time scale probed, which is longer than the lifetime of the dynamic bonds, thus leading to a viscoelastic liquid behavior. At higher frequencies, however, the experimental time is not long enough for the supramolecular interactions to dissociate, thus the polymers exhibit elastic-like behavior. Furthermore, the crossover frequency (ω_{cross}) between G' and G'' ($\tan \delta=1$) shifts to lower frequencies with the increase in covalent cross-linking density for all three samples. The lifetime of the reversible supramolecular networks can be measured as the inverse of the crossover frequency (ω_{cross}) of G' and G'' ($\tau=1/\omega$).⁶⁴ Thus, the supramolecular networks with higher covalent cross-linking density possess longer life time arising from the decrease of the polymer chain mobility, which is consistent with the DSC results.

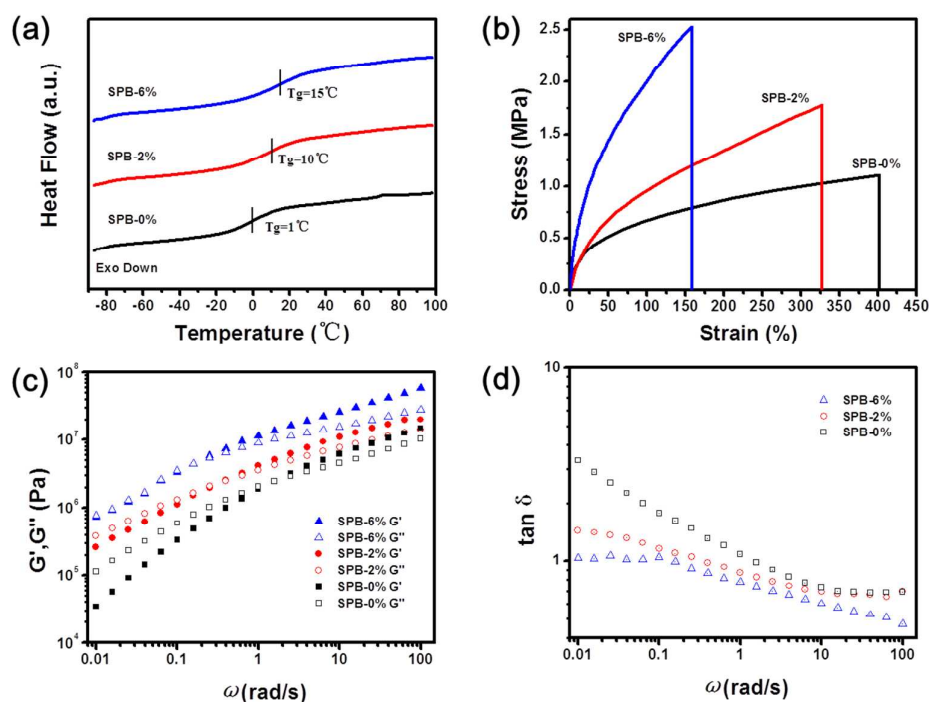


Fig. 3 (a) DSC thermograms, (b) stress-strain curves, and frequency dependence of (c) storage modulus (G'), loss modulus (G'') and (d) loss factor $\tan \delta$ (G''/G') of the polymers.

Table 1 Summary of the mechanical and self-healing properties of the resulting polymers. The average values were obtained with three samples.

Sample	Young's Modulus (MPa)	Elongation at break (%)	Stress at break (MPa)	Healing efficiency in 1 h (%)
SPB-0%	2.13±0.21	410±20	1.02±0.12	95±6
SPB-2%	3.15±0.03	322±26	1.78±0.18	72±5
SPB-6%	9.76±0.05	158±8	2.52±0.03	33±3

In contrast to common rubbers, the rubbers prepared exhibit unique self-healing properties at room temperature due to the existence of abundant dynamic ionic hydrogen bonds in the networks. To demonstrate this healing behavior, SPB-2% was cut at different positions with a razor blade, the fracture surfaces were then brought into contact. The damaged sample could spontaneously repair itself at room temperature without any external stimulus. After 1 h healing, the recovered sample can be stretched from 2 to 6 cm without breaking, as shown in Fig. 4a. The optical microscope illustrates that the cracks between the fracture surfaces were almost indiscernible after healing for 1 h (Fig. 4b), confirming the autonomic fusion of fracture surface as well as effective self-healing.

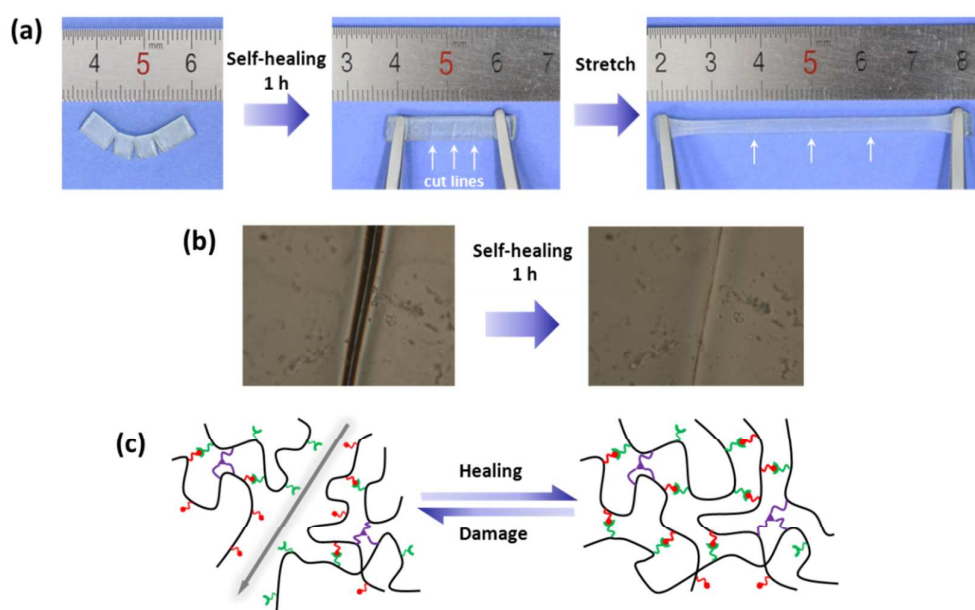


Fig. 4 (a) Photographs showing the self-healing behavior of SPB-2% sample. (b) Optical microscope

images of cut interfaces before and after healing. (c) Schematic illustration of the self-healing mechanism.

The mechanical properties of the samples healed as a function of healing time are shown in Fig. 5a-c. The stress-strain curves illustrate that the healing efficiency relies on the healing time. The sample SPB-0% without covalent cross-links exhibits the fastest healing speed, which can be healed to ~75% of its original strength in 5 min. About 93% of the original strength and 98% of the original extensibility are recovered after 1 h, indicating almost complete healing. A decrease in the healing efficiency was observed with the appearance of covalent cross-links in the system. This can be attributed to the irreversible covalent cross-links deter the mobility of polymer chains, thus resulting in the decrease in healing rate and efficiency. SPB-2% still possesses good self-healing capability, which was able to recover 77% of its original strength when healed for 1 h, and 90% after 12 h. For SPB-6%, it could only reach a healing efficiency of 35% even after 12 h. However, accelerated healing speed and increased healing efficiency could be realized at an elevated temperature. For example, the fracture surface in the SPB-6% was much better healed at 80 °C. This can be explained by the increased chain mobility at higher temperature due to the dissociation of ionic hydrogen bonds.

The unique self-healing property is attributed to the formation of dynamic ionic hydrogen bonds derived from acid-base reaction (Fig. 4c), which is similar to that of the reported dynamic non-covalent bonds based self-healing materials: upon mechanical damage, the non-covalent associations are more likely to break due to their lower strength compared to covalent bonds, resulting in the presence of a large number of reactive non-associated groups (COO^- or COOH , NH_3^+ or NH_2) on the fracture surfaces.⁸ Once the fracture surfaces being adjoined, the non-associated groups will react with each other and the broken ionic hydrogen bonds reformed at the interfaces assisted with the diffusion of polymer chains over time. Thus, the healing efficiency is higher at longer healing periods since more bonding bridges across the

interface are formed. In addition, for the amorphous polymers we studied, the low molecular weight and the relative low T_g allow the polymer chains to diffuse and rearrange at room temperature, further promoting the self-healing process. Thus, the polymer networks repair at room temperature without any external stimuli.

To confirm the proposed self-healing mechanism, the control sample CPB-6% with only covalent cross-links was prepared by photo-cross-linking of pristine PB with 6 wt% of trithiol cross-linker. It was found that the sample could not repair itself under the same conditions. In addition, polyamine was added on the fracture surfaces of SPB-2%, and the sample lost its self-healing capability owing to the competitive reaction between free COO^- or COOH groups with polyamine, further confirming that dynamic ionic hydrogen bonds are responsible for the self-healing properties.

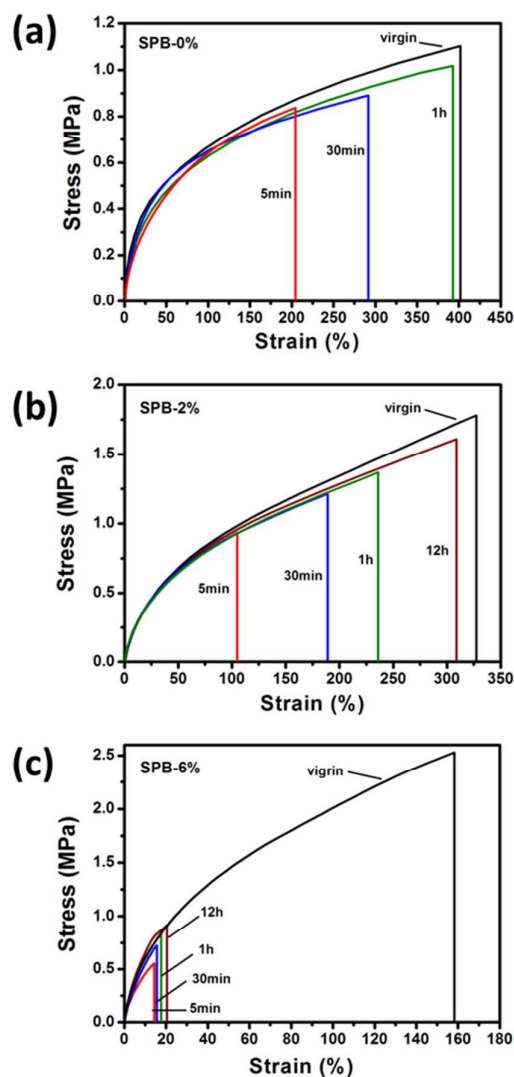


Fig. 5 Stress-strain curves of the (a) SPB-0%, (b) SPB-2% and (c) SPB-6% after different healing periods. The polymer films were cut into two separate pieces, and then brought into contact immediately, followed by healing for different times at room temperature.

Furthermore, an interesting thermally induced shape memory effect can be achieved by the incorporation of covalent cross-links. The shape-memory response of SPB-6% is shown in Fig. 6a. Herein, a permanent spiral-like SPB-6% film was prepared by photo-crosslinking of the film rolled on a glass rod. The film was deformed under heating at 60 °C, and then was cooled to fix the temporary flat shape. After

reheating to 60 °C, the film automatically recovered to its original spiral shape. The whole recovery process took place within several seconds, as shown in the Movie S1 in the Supporting Information. A proposed shape memory mechanism is shown in Fig. 6b. The thermal reversibility of ionic hydrogen bond is responsible for this thermally induced shape-memory behavior: upon heating, the dynamic ionic hydrogen bonds break, and then the materials can be deformed. When the deformed materials are cooled, the ionic hydrogen bonds reform, thus lock the temporary shape. Reheating will again break the reversible associations in the temporarily shaped sample, so the stored strain is released and the sample returns to the permanent shape driven by the recovery stress arising from the covalently cross-linked networks. In shape memory process, the covalent cross-links within polymer networks determine the permanent shape, while the ionic hydrogen bonds serve as reversible phase. The shape-memory behavior was achieved utilizing reversible cross-links to fix the temporary shape and covalent cross-links to recover its permanent shape.

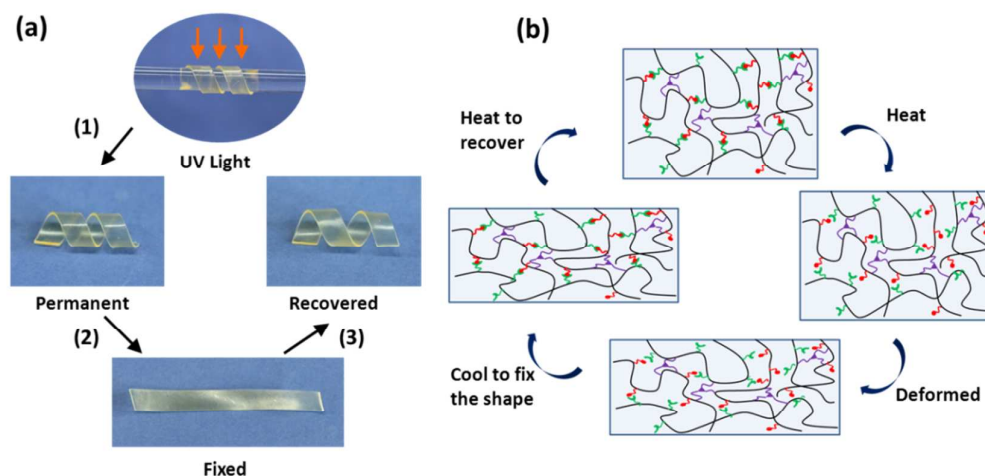


Fig. 6 (a) Photographs demonstrating the shape-memory behavior of SPB-6% film. (1) The film was set into a permanent spiral shape by wrapping the un-cross-linked film around a glass rod and irradiated with UV light, (2) heated to 60 °C while being deformed in a flat shape and then cooled to 20 °C to fix the temporary shape, (3) reheated to 60 °C to recover the permanent shape. (b) Proposed mechanism of thermally induced shape-memory behavior involving thermo-reversible ionic hydrogen bonds.

To better understand the shape memory mechanism, a temperature sweep containing consecutive thermal heating and cooling cycles was performed. Fig. 7a shows SPB-6% exhibits a reversible change in G' and G'' between -30 and 60 °C due to the reversible break and re-formation of ionic hydrogen bonds (results for SPB-0% and SPB-2% are shown in Fig. S2). To confirm the dynamic nature of ionic hydrogen bonds, the temperature sweep of covalently crosslinked CPB-6% as control sample was conducted to compare with the results of supramolecular polymer SPB-0% (Fig. S3). As can be seen, the sample CPB-6% behaves like an elastic network state with $G' > G''$ at higher temperature and displays a stable plateau of G' and G'' above 40 °C, indicating the thermal stability of covalent crosslinks. In contrast, the supramolecular polymer SPB-0% shows a drastic decrease in G' and G'' as the temperature increases and a transition from an elastic-like behavior ($G' > G''$) to liquid-like behavior ($G' < G''$) occurs at 31 °C, thus confirming that the drastic decrease in the modulus is due to the dissociation of ionic hydrogen bonds with increasing temperature. The drastic change in the modulus with temperature is considered to be the significant factor to achieve the thermal shape memory effect.^{65,66} To investigate the shape-memory properties of the sample, a typical thermal one-way shape-memory cycle for SPB-6% is shown in Fig. 7b. The sample was first heated to 60 °C, and a stress of 0.03 MPa was applied. Then the strain was fixed by cooling the sample to 10 °C, after which the stress was removed. Shape recovery was achieved by reheating the sample to 60 °C and cooling back to 10 °C afterwards. The sample showed both high strain fixing value (R_f) of ~95% and recovery value (R_r) of ~99%, exhibiting excellent shape-memory properties. Furthermore, the fixing and recovery ratios stay consistent even after many cycles (Fig. S4), showing good cycle lifetime for the material. The effect of covalent cross-linking density on the shape memory properties was also studied. The thermal shape-memory cycle for SPB-2% is shown in Fig. S5. The fixing stays relatively constant with R_f of ~96%, while R_r decreases to ~82%. This is more likely due to the

residual strain resulted by slipping between the polymer chains at higher temperature for the polymers with low covalent cross-linking density.

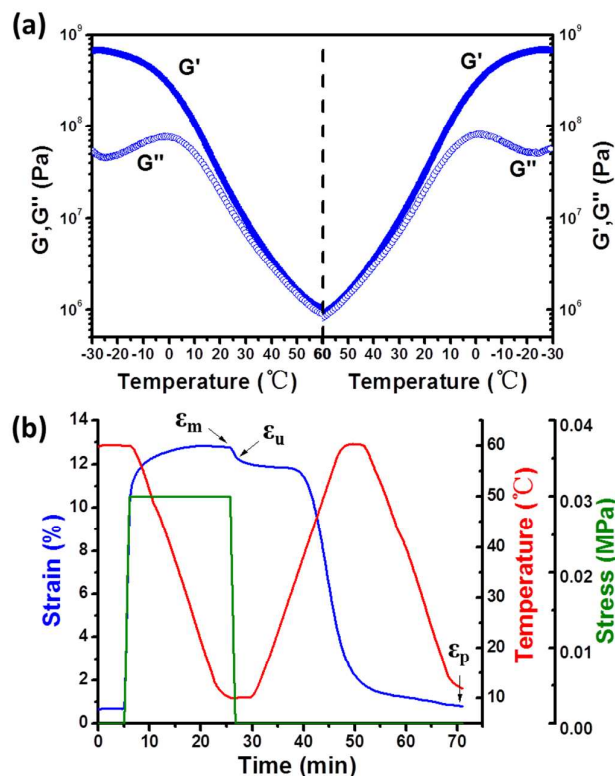


Fig. 7 (a) G' and G'' of SPB-6% during heating-cooling cycle between -30 and 60 °C, measured at $\omega = 10$ rad/s, $\gamma = 0.03$ % from -30 to -10 °C and $\gamma = 0.1$ % from -10 to 60 °C. (b) Typical thermal one-way shape-memory cycle for SPB-6%.

4 Conclusion

In summary, a novel thermo-reversible rubber is constructed by the thiol-ene functionalized polybutadiene oligomers via dynamic ionic hydrogen bonds and covalent cross-links. In the resultant rubbers, the covalent cross-links form a permanent network which can enhance the mechanical strength and maintain the shape of the polymers, while the dynamic ionic hydrogen bonds construct a reversible network which can increase the toughness, realize self-healing as well as shape-memory function. By

varying the covalent cross-linking density, the mechanical properties and the stimuli-responsive behavior can be systematically tuned. In contrast to conventional rubbers, the rubbers prepared exhibit adjustable stimuli-responsive behavior in combination with excellent mechanical performance, which facilitate their application as multifunctional smart materials. This work demonstrates a simple and effective pathway to fabricate multifunctional polymer with desired functions, and the strategy can also be extended to explore other type of dynamic non-covalent or covalent interactions to access a new range of multi-responsive properties.

Acknowledgements

This work was financially supported by the National Natural Science Foundation of China (NSFC) (U1134105, 21421061) and Ministry of Science and Technology of China (MOST) (2012CB933800).

Notes and references

- 1 L. Brunsveld, B. J. B. Folmer, E. W. Meijer and R. P. Sijbesma, *Chem. Rev.*, 2001, **101**, 4071-4097.
- 2 B. Rybtchinski, *ACS Nano*, 2011, **5**, 6791-6818.
- 3 X. Yan, F. Wang, B. Zheng and F. Huang, *Chem. Soc. Rev.*, 2012, **41**, 6042-6065.
- 4 A. Noro, M. Hayashi and Y. Matsushita, *Soft Matter*, 2012, **8**, 6416-6429.
- 5 K. Liu, Y. Kang, Z. Wang and X. Zhang, *Adv. Mater.*, 2013, **25**, 5530-5548.
- 6 A. W. Bosman, R. P. Sijbesma and E. W. Meijer, *Mater. Today*, 2004, **7**, 34-39.
- 7 C. X. Sun, M. A. J. van der Mee, J. G. P. Goossens and M. van Duin, *Macromolecules*, 2006, **39**, 3441-3449.
- 8 P. Cordier, F. Tournilhac, C. Soulie-Ziakovic and L. Leibler, *Nature*, 2008, **451**, 977-980.
- 9 M. Burnworth, L. Tang, J. R. Kumpfer, A. J. Duncan, F. L. Beyer, G. L. Fiore, S. J. Rowan and C.

- Weder, *Nature*, 2011, **472**, 334-337.
- 10 F. Herbst, D. Dohler, P. Michael and W. H. Binder, *Macromol. Rapid Commun.*, 2013, **34**, 203-220.
- 11 C. Yu, C.-F. Wang and S. Chen, *Adv. Funct. Mater.*, 2014, **24**, 1235-1242.
- 12 X. Xing, L. Li, T. Wang, Y. Ding, G. Liu and G. Zhang, *J. Mater. Chem. A.*, 2014, **2**, 11049-11053.
- 13 G. Liu, C. Guan, H. Xia, F. Guo, X. Ding and Y. Peng, *Macromol. Rapid Commun.*, 2006, **27**, 1100-1104.
- 14 C. Liu, H. Qin and P. T. Mather, *J. Mater. Chem.*, 2007, **17**, 1543-1558.
- 15 M. Behl, M. Y. Razzaq and A. Lendlein, *Adv. Mater.*, 2010, **22**, 3388-3410.
- 16 T. Pretsch, *Polymers*, 2010, **2**, 120-158.
- 17 L. Sun, W. M. Huang, Z. Ding, Y. Zhao, C. C. Wang, H. Purnawali and C. Tang, *Mater. Des.*, 2012, **33**, 577-640.
- 18 G. J. Berg, M. K. McBride, C. Wang and C. N. Bowman, *Polymer*, 2014, **55**, 5849-5872.
- 19 Q. Wang, Y. Bai, Y. Chen, J. Ju, F. Zheng and T. Wang, *J. Mater. Chem. A.*, 2015, **3**, 352-359.
- 20 R. Yerushalmi, A. Scherz, M. E. van der Boom and H.-B. Kraatz, *J. Mater. Chem.*, 2005, **15**, 4480-4487.
- 21 S. L. Li, T. Xiao, C. Lin and L. Wang, *Chem. Soc. Rev.*, 2012, **41**, 5950-5968.
- 22 X. Yan, D. Xu, X. Chi, J. Chen, S. Dong, X. Ding, Y. Yu and F. Huang, *Adv. Mater.*, 2012, **24**, 362-369.
- 23 S. Dong, B. Zheng, Y. Yao, C. Han, J. Yuan, M. Antonietti and F. Huang, *Adv. Mater.*, 2013, **25**, 6864-6867.
- 24 M. Guo, L. M. Pitet, H. M. Wyss, M. Vos, P. Y. Dankers and E. W. Meijer, *J. Am. Chem. Soc.*, 2014, **136**, 6969-6977.
- 25 H. Koerner, G. Price, N. A. Pearce, M. Alexander and R. A. Vaia, *Nat. Mater.*, 2004, **3**, 115-120.

- 26 J. W. Cho, J. W. Kim, Y. C. Jung and N. S. Goo, *Macromol. Rapid Comm.*, 2005, **26**, 412-416.
- 27 G. Fei, C. Tuinea-Bobe, D. Li, G. Li, B. Whiteside, P. Coates and H. Xia, *RSC Adv.*, 2013, **3**, 24132-24139.
- 28 M. Y. Razzaq, M. Behl and A. Lendlein, *Adv. Funct. Mater.*, 2012, **22**, 184-191.
- 29 M. Y. Razzaq, M. Behl, K. Kratz and A. Lendlein, *Adv. Mater.*, 2013, **25**, 5730-5733.
- 30 Y. Feng, H. Zhao, S. Zhang, L. Jiao, J. Lu, H. Wang and J. Guo, *Macromol. Symp.*, 2011, **306-307**, 18-26.
- 31 A. Lendlein and R. Langer, *Science*, 2002, **296**, 1673-1676.
- 32 C. Wischke and A. Lendlein, *Pharm. Res.*, 2010, **27**, 527-529.
- 33 M. Ecker and T. Pretsch, *RSC Adv.*, 2014, **4**, 286-292.
- 34 M. Ecker and T. Pretsch, *RSC Adv.*, 2014, **4**, 46680-46688.
- 35 C. C. Wang, W. M. Huang, Z. Ding, Y. Zhao, H. Purnawali, L. X. Zheng, H. Fan and C. B. He, *Smart Mater. Struct.*, 2012, **21**, 115010-115018.
- 36 X. Luo and P. T. Mather, *ACS Macro Lett.*, 2013, **2**, 152-156.
- 37 Y. Heo and H. A. Sodano, *Adv. Funct. Mater.*, 2014, **24**, 5261-5268.
- 38 Z. Wang, W. Fan, R. Tong, X. Lu and H. Xia, *RSC Adv.*, 2014, **4**, 25486-25493.
- 39 X. Lu, G. Fei, H. Xia and Y. Zhao, *J. Mater. Chem. A.*, 2014, **2**, 16051-16060.
- 40 S. Chen, F. Mo, Y. Yang, F. J. Stadler, S. Chen, H. Yang and Z. Ge, *J. Mater. Chem. A.*, 2015, **3**, 2924-2933.
- 41 J. Li, J. A. Viveros, M. H. Wrue and M. Anthamatten, *Adv. Mater.*, 2007, **19**, 2851-2855.
- 42 J. Li, C. L. Lewis, D. L. Chen and M. Anthamatten, *Macromolecules*, 2011, **44**, 5336-5343.
- 43 J. R. Kumpfer and S. J. Rowan, *J. Am. Chem. Soc.*, 2011, **133**, 12866-12874.
- 44 I. Mora-Barrantes, M. A. Malmierca, J. L. Valentin, A. Rodriguez and L. Ibarra, *Soft Matter*, 2012, **8**,

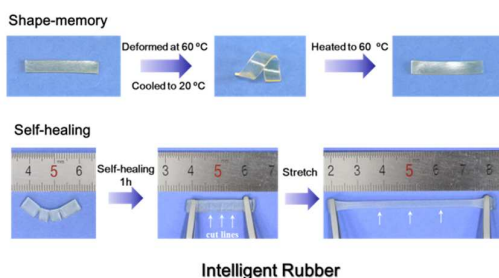
- 5201-5213.
- 45 S. P. Khor, R. J. Varley, S. Z. Shen and Q. Yuan, *J. Appl. Polym. Sci.*, 2013, **128**, 3743-3750.
- 46 D. C. Tuncaboylu, A. Argun, M. P. Algi and O. Okay, *Polymer*, 2013, **54**, 6381-6388.
- 47 C. Wang, N. Liu, R. Allen, J. B. Tok, Y. Wu, F. Zhang, Y. Chen and Z. Bao, *Adv. Mater.*, 2013, **25**, 5785-5790.
- 48 C. L. Lewis, K. Stewart and M. Anthamatten, *Macromolecules*, 2014, **47**, 729-740.
- 49 M. Meot-Ner, *Chem. Rev.*, 2005, **105**, 213-284.
- 50 K. Sada, T. Tani and S. Shinkai, *Synlett*, 2006, **2006**, 2364-2374.
- 51 E. Yashima, T. Matsushima and Y. Okamoto, *J. Am. Chem. Soc.*, 1997, **119**, 6345-6359.
- 52 K. C. F. Leung, P. M. Mendes, S. N. Magonov, B. H. Northrop, S. Kim, K. Patel, A. H. Flood, H.-R. Tseng and J. F. Stoddart, *J. Am. Chem. Soc.*, 2006, **128**, 10707-10715.
- 53 A. Aboudzadeh, M. Fernandez, M. E. Munoz, A. Santamaria and D. Mecerreyes, *Macromol. Rapid Commun.*, 2014, **35**, 460-465.
- 54 M. A. Aboudzadeh, M. E. Munoz, A. Santamaria, R. Marcilla and D. Mecerreyes, *Macromol. Rapid Commun.*, 2012, **33**, 314-318.
- 55 M. A. Aboudzadeh, M. E. Muñoz, A. Santamaría, M. J. Fernández-Berridi, L. Irusta and D. Mecerreyes, *Macromolecules*, 2012, **45**, 7599-7606.
- 56 K. S. Partridge, D. K. Smith, G. M. Dykes and P. T. McGrail, *Chem. Commun.*, 2001, 319-320.
- 57 A. Noro, M. Hayashi, A. Ohshika and Y. Matsushita, *Soft Matter*, 2011, **7**, 1667-1670.
- 58 A. Noro, K. Ishihara and Y. Matsushita, *Macromolecules*, 2011, **44**, 6241-6244.
- 59 L. Zhang, L. R. Kucera, S. Ummadisetty, J. R. Nykaza, Y. A. Elabd, R. F. Storey, K. A. Cavicchi and R. A. Weiss, *Macromolecules*, 2014, **47**, 4387-4396.
- 60 N. ten Brummelhuis, C. Diehl and H. Schlaad, *Macromolecules*, 2008, **41**, 9946-9947.

- 61 J. Yuan, N. ten Brummelhuis, M. Junginger, Z. Xie, Y. Lu, A. Taubert and H. Schlaad, *Macromol. Rapid Commun.*, 2011, **32**, 1157-1162.
- 62 Y. Yang and M. W. Urban, *Chem. Soc. Rev.*, 2013, **42**, 7446-7467.
- 63 Y. Bai, Y. Chen, Q. Wang and T. Wang, *J. Mater. Chem. A.*, 2014, **2**, 9169-9177.
- 64 K. E. Feldman, M. J. Kade, E. W. Meijer, C. J. Hawker and E. J. Kramer, *Macromolecules*, 2009, **42**, 9072-9081.
- 65 C. Bilici and O. Okay, *Macromolecules*, 2013, **46**, 3125-3131.
- 66 U. Gulyuz and O. Okay, *Macromolecules*, 2014, **47**, 6889-6899.

Table of contents entry

Intelligent Rubber with Tailored Properties for Self-healing and Shape Memory

Dong Wang, Jing Guo, Huan Zhang, Beichen Cheng, Heng Shen, Ning Zhao,* and Jian Xu*



Thermoreversible rubbers are prepared by the thiol-ene functionalized polybutadiene oligomers via dynamic ionic hydrogen bonds and covalent cross-links, exhibiting tailored properties for self-healing and shape memory functions.